Vertical Velocity Characteristics of Deep Convection over Darwin, Australia

PETER T. MAY

Bureau of Meteorology Research Centre, Melbourne, Victoria, Australia

DEEPAK K. RAJOPADHYAYA

Cooperative Institute for Research in Environmental Science, University of Colorado, Boulder, Colorado

(Manuscript received 26 January 1998, in final form 16 June 1998)

ABSTRACT

Continuous vertical velocity measurements using a 50-MHz wind profiler located at Darwin in northern Australia during periods of active convection have been analyzed. This dataset is dominated by continental-type convection. Numerous examples of shallow, deep, and decaying convection were seen and it is shown that only the deep systems have substantial tilts to the draft structure. The most intense updrafts occur above the freezing level, but shallow convection also produces large-amplitude vertical motions. The strength of these updrafts in this dataset is very similar to other tropical, oceanic data. That observation is consistent with the idea that the magnitude of the updrafts is much less in the Tropics than for intense midlatitude convection because the convective available potential energy is distributed over a much deeper layer in the Tropics, although more intense updrafts may be present at other tropical locations, such as the Tiwi Islands north of Darwin. The size of the cores, however, is significantly greater here than with oceanic data and is similar to midlatitude results, thus supporting the suggestion that boundary layer depth is important in determining the horizontal scale. There is a net detrainment in the upward cores above the freezing level occurring at all space scales. The mass flux in intense updrafts is almost constant with height below the freezing level but is almost cancelled by downdrafts and the immediate surrounding environment. Two populations of downdrafts are seen, one a dynamical response associated with intense updrafts at all heights and a second driven by precipitation processes below the freezing level. The core size, intensity, and mass flux are all approximately lognormally distributed. It is shown that a wide range of velocity and size scales contribute to the upward mass flux.

1. Introduction

The Australian Bureau of Meteorology and the Aeronomy Laboratory of the National Oceanic and Atmospheric Administration have been operating a 50-MHz wind profiler at Darwin, Australia, since 1989. During the first year of operation it was only measuring the vertical wind component. Data from the entire 1989–90 wet season have been examined and 29 events of active convection over the profiler have been identified. This continuous high-resolution dataset lends itself to a statistical analysis comparable with and complementing aircraft-based studies such as LeMone and Zipser (1980), Jorgensen et al. (1985), Lucas et al. (1994), and others. The dataset contains examples of essentially all stages of the growth of convective systems, with examples of shallow convection only a few kilometers deep, more intense isolated cells reaching near the freezing level, deep mature cells with extensive convective downdrafts and new cells forming on the cold pool outflows, and cells that are clearly transitioning into a stratiform mesoscale up-/downdraft pattern. These data have been analyzed to investigate the statistics of the intense cores within convective clouds. This dataset also includes extensive periods of stratiform and decaying precipitation systems and these will be the focus of further work.

Storms in Darwin occur during a wide variety of shear/convective available potential energy (CAPE) conditions (Keenan and Carbone 1992). Darwin experiences two distinct types of convection during the wet season. During the monsoon period, where there are low-level westerly winds, the convection is oceanic in character. The storms sampled during this period are similar to those sampled over the ocean in the Equatorial Mesoscale Experiment (EMEX). In the buildup to the monsoon (transition period) and during break periods, the low-level winds are easterly. Convection during these periods is more continental in character. These include storms developing on sea-breeze convergence lines and well-organized intense squall lines that prop-

Corresponding author address: Dr. P. T. May, Bureau of Meteorology Research Centre, GPO Box 1289K, Melbourne, Victoria 3001, Australia.
E-mail: p.may@bom.gov.au

agate from inland (Keenan and Carbone 1992). Radar studies have generally led to the expectation that break period storms are more intense; they are generally much more organized. Here we define the monsoon periods as those with an 850-hPa westerly wind component (Holland 1986), but the separation of cases does not alter for layer-averaged definitions (Drosdowsky 1996). Most of these profiler data were collected under break and transition conditions (25 of 29 cases) as the monsoon that year was very brief (Rutledge et al. 1992).

Radar wind profilers have been used to study vertical motions in convective systems in the past (e.g., Balsley et al. 1988). These include the dual-frequency observations of Chilson et al. (1993) focusing on the character of precipitation echoes in deep convection and the study of May and Rajopadhyaya (1996, 1997), which examined the vertical velocity and precipitation characteristics of a squall line in some detail. This latter study also includes diagnostics of heating rates implied by the system vertical motion field and the balance between vertical motion and changes in the precipitation characteristics in the stratiform part of a squall line. The studies of Cifelli and Rutledge (1994, 1998) analyzed a number of storm systems and the characteristics of individual storm case studies and storm composites were related to the precipitation type and the characteristics of storms in the monsoon and break season rainfall regimes. These papers found some significant differences in the mean vertical motion profile between monsoon and break storms, with evidence of a double peak in the vertical motion profile associated with warm rain (lower peak) and glaciation and a decrease in precipitation loading (upper peak) for break cases, while the monsoon cases had a more uniform profile. However, the number of cases was relatively small compared with the sample analyzed in this paper.

There have been many aircraft-based studies of convection. These range from studies of the vertical velocity characteristics of fair weather cumulus (Malkus 1955) to the pioneering work of the Thunderstorm Project (Byers and Braham 1949), investigating deep intense convection over the Midwest of the United States and Florida, and hurricane vertical motions (Gray 1965). The classic papers of LeMone and Zipser (1980) and Zipser and LeMone (1980) presented a detailed statistical study of the draft and core characteristics based on numerous aircraft penetrations of convective towers at various heights during the Global Atmospheric Research Program (GARP) Atlantic Tropical Experiment (GATE). More recent studies have contrasted the GATE and Thunderstorm Project data with convection over other oceanic basins, such as north of Australia and the Gulf of Carpentaria during EMEX (Jorgensen and LeMone 1989; Lucas et al. 1994). These analyses provide a benchmark for comparisons with the profiler data. The data to be analyzed here sample a similar number of convective cores (to be defined in the next section) but are dominated by continental tropical convection. One advantage of the profiler data is the continuous height coverage, so that the vertical extent and coherence of the cores can be studied in addition to the statistics at each level. These correlation structures can be compared with those obtained in tropical cyclones using airborne radar by Black et al. (1996).

Vertical motions within convective systems have been extensively studied on a case study basis (e.g., Heymsfield and Schotz 1985). Yuter and Houze (1995a,b,c) analyzed the statistical characteristics of the vertical motions and reflectivity field within a convective complex during the Convection and Precipitation/Electrification Experiment (CAPE), using dual–Doppler radar analyses in detail. This included the temporal evolution of the fields from a developing stage through to a decay phase. The general characteristics of their results will be compared and contrasted with the data over many events here.

2. Observations

The 50-MHz wind profiler was operating in a vertical-only mode during the 1989–90 wet season at Darwin. It was sampling the height region between 1.7 and 20 km, but the highest quality data were limited to heights below 11 km. The height resolution of the observations was 1 km, but data were sampled every 500 m. The time resolution was 86 s. The resulting Doppler spectra were then stored for reanalysis.

The profilers measure the radar backscatter from both turbulent irregularities (giving an estimate of the vertical wind) and precipitation particles (both rain and ice; e.g., Fukao et al. 1985; Larsen and Rottger 1987; Wakasugi et al. 1986; May 1991; Chilson et al. 1993). The profiler spectra have been reanalyzed to remove the effects of precipitation echoes from the estimates of the mean vertical motion. A least squares fit of a Gaussian function is fitted to the ''clear air'' part of the spectrum. Figure 1 shows a typical example of several of the spectra and the corresponding velocity estimate seen in deep convection. These velocity estimates were then manually edited and sometimes reanalyzed to ensure that biases associated with the precipitation echoes have been removed.

Periods with vertical motions with an amplitude greater than 1.5 m s^{-1} have been identified and are defined here as convective cores. For our purposes, this threshold value provides a signature of convective precipitation that has been selected for this analysis. This somewhat loose definition is almost equivalent to the definitions of Houghton (1968) and Houze (1981) and corresponds to velocities greater than the typical fall speed of ice crystals and aggregates. A lower limit of 1 m s^{-1}, as used by LeMone and Zipser (1980), allowed ''cores'' that were clearly internal waves to appear, but the basic results presented here are similar if a low limit is chosen. In most cases these waves were in the clear air and were coherent over several km (typically from

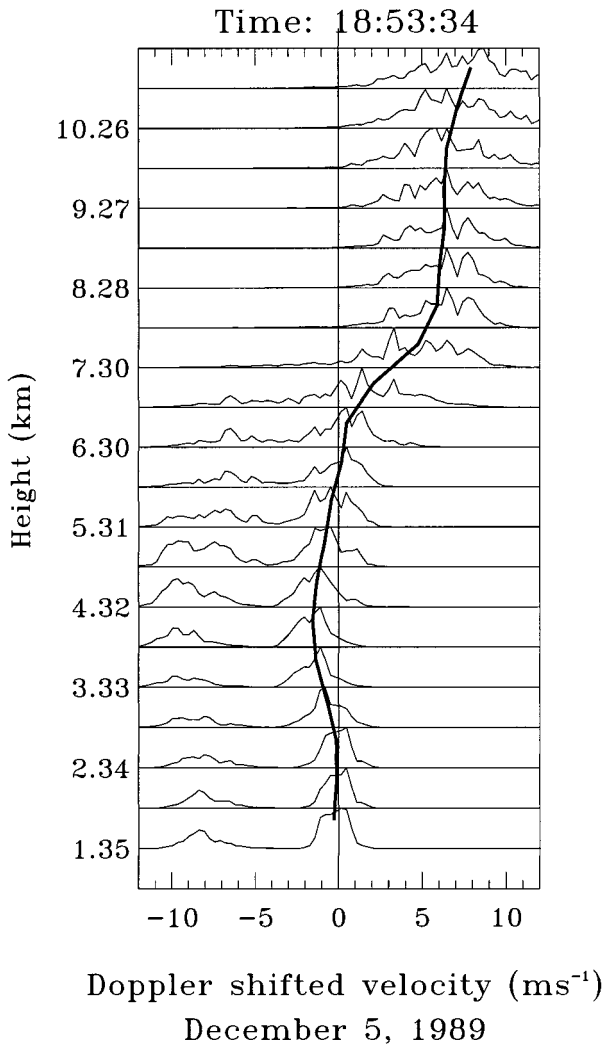

FIG. 1. Example of profiler Doppler spectra and associated velocity estimates (solid line). The spectral peaks with large downward motions are rain echoes (after May and Rajopadhyaya 1996).

4 to above 10 km) and over many cycles with very little phase change with height. This implies that the waves were propagating almost vertically and the frequency of the oscillations were typically near the Brunt–Väisälä frequency. Examples of these types of oscillations can be found in May et al. (1995). However, particularly in the case of downdrafts, there are some cases where there is coherent vertical motion over a large depth, but this threshold may produce several disjointed cores. An example of this is the deep descending motion next to the deep mature cells during the 5 December 1989 squall line case analyzed by May and Rajopadhyaya (1996).

One limitation of the present study is that the profiler data cannot be used to differentiate between nonprecipitating clouds and clear air. So, for example, intense downdrafts may or may not be in cloudy air. Similar observations to these with a collocated cloud radar could be used to answer some questions that arise in this dataset.

In order to compare the slopes of the systems and compare scale sizes estimated from aircraft and the time sections from the profiler, a time-to-space-scale conversion is needed. Keenan and Carbone (1992) studied several convective systems over Darwin and found a mean speed of 10 m s^{-1} with a standard deviation of 3 m s^{-1}. They prepared a table showing speed of movement of storms (c) against the 700-hPa wind (u_{700}). A regression line has been fitted to the data. Using all the data a regression is obtained, $c = 4.2 + 0.59u_{700}$, with a standard deviation of 3.7 m s^{-1} and a correlation coefficient of 0.449, suggesting a constant value may give better results. However, if three outlying values are removed, a fit of $c = 1.7 + 0.69u_{700}$ is obtained with a standard deviation of 1.95 m s^{-1} and a correlation coefficient of 0.775. This latter equation is used here to convert the temporal scale of the profiler to a spatial scale for comparison with aircraft data. The 86-s sampling of the profiler data is equivalent to a spatial resolution of about 600–1100 m, similar to the LeMone and Zipser core definition.

These profiler data are clearly complementary to the aircraft observations of LeMone and Zipser and others since (e.g., Lucas et al. 1994; Black et al. 1996). The profiler is limited to a temporal sampling of a single location but has the advantage of continuous height coverage, so that the vertical coherence of the draft structure can be evaluated, although three-dimensional effects mean that our measure of the vertical coherence is a lower limit to the true vertical extent. With this sampling it is difficult to create a similar definition of LeMone and Zipser's drafts ($w > 0$ m s^{-1} for 500 m, >0.5 m s^{-1} for >100 m), but, in the convective areas analyzed, the period for downward velocities greater than 0.1 m s^{-1} is about 60% greater than for upward velocities greater than 0.1 m s^{-1} below the freezing level (FZL, $\sim$4.5 km), and the ratio decreases above this to about 30% at 10 km. This is broadly consistent with the Zipser and LeMone (1980) result that the area of downdrafts was about twice that of updrafts.

3. Time–height sections

Twenty-nine time–height sections of the vertical velocity have been examined and can be classified according to three fairly distinct categories. These are ''shallow'' convection, where the cores may reach as high as 8 km ($\sim$3 km above the FZL), but do not show a distinct acceleration above the FZL. This is consistent with the notion that these shallow cells are associated with warm rain processes; glaciation, with its concomitant release of latent heat, has not occurred to an extent sufficient to support a deep convective core. Deep systems have cores extending above 10 km and typically show acceleration above the FZL. These systems may also contain new cells growing ahead of the deep mature

TABLE 1. Storm characteristics and sounding data.

Date	Time (LT)	Duration (min)	$u700$	$\phi 700$	Slope (°)	CAPE (J kg^{-1})	Surface-700 hPa wind shear ($\times$ 0.001 s^{-1})
Shallow cases							
3 Dec 1989	12:50	15	5	110	76	1348	3.3
8 Dec 1989	14:45	20	12	100	35	1269	4.0
12 Dec 1989	15:35	86	7	110	80	1405	2.9
1 Jan 1990	18:20	15	17	110	67	663	5.8
18 Jan 1990	19:10	60[a]	9	90	90	361	0.3
22 Jan 1990	20:15	40	4	150	90	1185	1.5
28 Jan 1990	22:15	25	8	90	74	806	4.9
31 Jan 1990	16:35	190[a]	5	70	88	366	1.7
2 Feb 1990	12:45	15	6	100	85	2917	1.4
9 Feb 1990	12:18	12	12	100	90	948	4.0
19 Feb 1990	15:05	5	12	80	90	1561	4.3
28 Feb 1990	15:35	10	7	90	63	345	0.7
3 Mar 1990	22:35	8	13	130	43	3416	1.3
Deep cases							
5 Dec 1989	18:10	50	12	150	23	575	3.7
15 Dec 1989	10:00	30	4	240 M	62	1996	1.0
12 Jan 1990	18:00	25	5	280 M	60	380	2.5
13 Jan 1990	19:40	60	4	340 M	74	1066	1.7
8 Feb 1990	15:40	40	15	100	43	2758	4.1
19 Feb 1990	19:50	50	12	90	28	1561	4.3
24 Feb 1990	16:15	30	9	25	60	876	3.0
2 Mar 1990	20:55	30[b]	8	130	53	2470	1.9
Decaying cases							
11 Dec 1989	13:20	30	8	70	0	1074	2.0
28 Dec 1989	16:05	15	8	110	65	2561	4.7
20 Jan 1990	6:20	140[a]	3	90	74	827	0.7
23 Jan 1990	16:20	20[c]	8.5	120	85	415	3.1
22 Feb 1990	14:40	60[c]	9	130	38	2411	2.1
3 Mar 1990	23:00	50[c]	14	120	23	3416	1.3
8 Mar 1990	16:50	10	8	210 M	85	752	3.0
11 Mar 1990	7:40	45	9	120	33	284	3.4

[a] Denote long period; actually contains 2 or more short active periods.
[b] This event was longer but had a power failure at the profiler. The record was stopped after last complete core.
[c] These decay cases also contained a shallow cell developing ahead of larger decaying cells.
M: Monsoonal case as defined by a 700-hPa westerly wind component.

cells where warm rain processes are also dominating (e.g., Cifelli and Rutledge 1994; May and Rajopadhyaya 1996). The third category is where the dominant cell over the profiler is decaying and a more stratiform circulation of an up–downdraft couplet is visible, although the amplitude of the vertical motions is still several meters per second. In these instances the downdraft may be of the order of the horizontal dimension of the convective cell (cf. Knupp 1987). These definitions are subjective and are not always clear-cut. For example, two of the shallow cases have very small and weak upper-level cores well behind the main shallow cases, which have some resemblance to the ''decaying'' definition, and likewise, two of the decay cases have small shallow cells ahead that are similar to some of the ''deep'' cases. There are 13 cases of shallow convection, 8 of deep convection, and 8 where the convection appears to be decaying. These classifications illustrate the life cycle of the convective systems, with the shallow cases being convection-forming near the coastal regions. The relatively high number of decaying systems may be a result of the frequent occurrence of squall lines forming on the higher ground to the east and south of Darwin during the break and transition periods and decaying as they approach Darwin (Keenan and Carbone 1992; Rasmussen and Rutledge 1993).

Table 1 lists the events, their duration and the values of CAPE,[1] and the low-level wind shear from the 1000 UTC (1830 LT) soundings on the day of the event. The shear is defined as the magnitude of the surface to 700-hPa shear. The height is chosen as it is close to the maximum height of the easterly wind in the transition

[1] CAPE $= \int_{z1}^{z2} g(\theta_c - \theta_{env})/\theta_{env}\, dz$, where g is the acceleration due to gravity, θ_c is the potential temperature of a parcel taken from the surface, θ_{env} is the potential temperature of the environment, $z1$ is the level of free convection, and $z2$ is the equilibrium level.

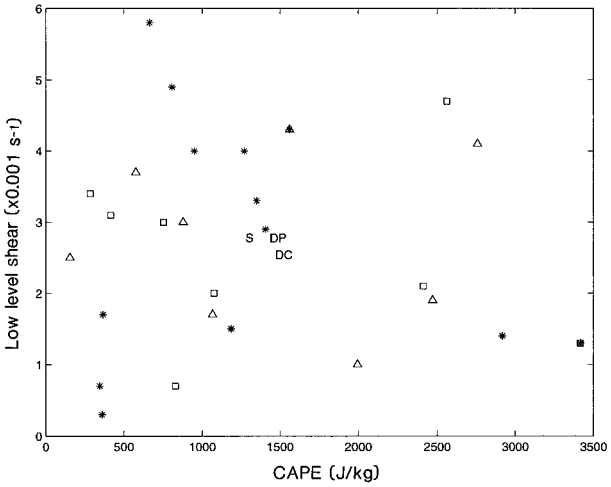

FIG. 2. Scatterplot of CAPE and surface to 700-hPa wind shear for each event listed in Table 1. The data for shallow cases are marked as *, deep cases as △, and decaying cases as □. The mean values for all the shallow (S), deep (DP), and decaying (DC) cases are also marked.

and break seasons and is similar to the maximum westerlies during the monsoon period (cf. Keenan and Carbone 1992). The storms occur over a wide range of shear and CAPE conditions as previous studies have found (Keenan and Carbone 1992). This is summarized in Fig. 2. The means for each category are shown in this figure and are not significantly different from each other. Similar conclusions apply to the median and standard deviations of the shear and CAPE for each category. The mean 700-hPa wind speed for the different categories are also similar. Of course, the classifications apply only to the system that passes over the profiler, and other types of systems than those over the profiler may coexist in the area.

a. Shallow convection

The shallow convection with little or no penetration above the FZL implies that warm rain processes are dominant. This category shows the most variation in many respects. There are several examples of shallow systems that do not reach the FZL and some where the cores penetrate higher. Figure 3a shows a series of very shallow cells. These cells are very regularly spaced but are precipitating and only extend a short height into the free troposphere (the top of the boundary layer is ~1.5–2 km AGL). This high degree of organization may be some self-organization between boundary layer convection in a potentially moist unstable atmosphere with gravity wave activity in the free troposphere (e.g., Kuettner et al. 1987) although there is little evidence of strong gravity wave activity aloft. The 2D [lagged in time (min) and height (km)] autocorrelation function of this velocity field is also shown. This highlights the erect and repetitive nature of the cells in this example. The correlation functions only ever become slightly negative in these cases, although large negative correlations do occur for cases of well-defined internal wave trains that have been excluded from these datasets.

A more typical example of this category is shown in Fig. 3b. Here the intense updraft extends to just above the FZL with velocities exceeding 6 m s^{-1}. Of particular note is the downdraft just next to the upward core. This is in a precipitation-free region and both precipitation loading and evaporation seem unlikely explanations of this, although the downdraft may be in-cloud and detrainment of cloud water from the upward core may allow these processes to occur. The close association of downward cores near intense upward cores is a ubiquitous feature at all heights. It may be associated with the initiation of a gravity wave by the displacement of air by the core and intense heating associated with such strong vertical motions (there is some evidence of a wave effect ahead of the main core in this example), or it may be a response to nonhydrostatic pressure perturbations associated with the rapid accelerations (e.g., Yuter and Houze 1995b). We will return to this question in a moment. Again, the correlation function illustrates the erect nature of these cores, which are coherent over several kilometers.

The erect updrafts are further illustrated by the autocorrelation function of all the shallow cases (Fig. 4) and the values of the slopes for each case given in Table 1. The high correlation values are almost solely induced by the upward cores for these examples. If the correlation function of only downward cores were used, there would be little coherence. The erect structure is consistent with many relatively short-lived cells, in contrast with the deep systems with tilted updrafts to be discussed next, which are usually associated with long-lived squall lines and convective complexes. However, radar data show that several of the shallow cases occurred near the edge of larger well-organized systems. Some light rain was observed in the profiler spectra following about half of the cases; but for one exception, these were the cases with the largest tilts and, in that case, the squall was mostly made up of shallow cells.

b. Deep convection

A typical example of a time–height section through a deep convective cell is shown in Fig. 5. A feature to note here is the acceleration above the FZL as glaciation releases latent heat and precipitation loading decreases. A spectral peak corresponding to supercooled water is often seen in these cores extending several kilometers above the FZL (May and Rajopadhyaya 1996). Velocities exceeding 10 m s^{-1} occur. This example shows a very coherent and strong convective downdraft behind the upward core. Other examples show similar features and several show new convection forming ahead of the deep mature cell (e.g., May and Rajopadhyaya 1996). The downdraft is associated with both precipitation

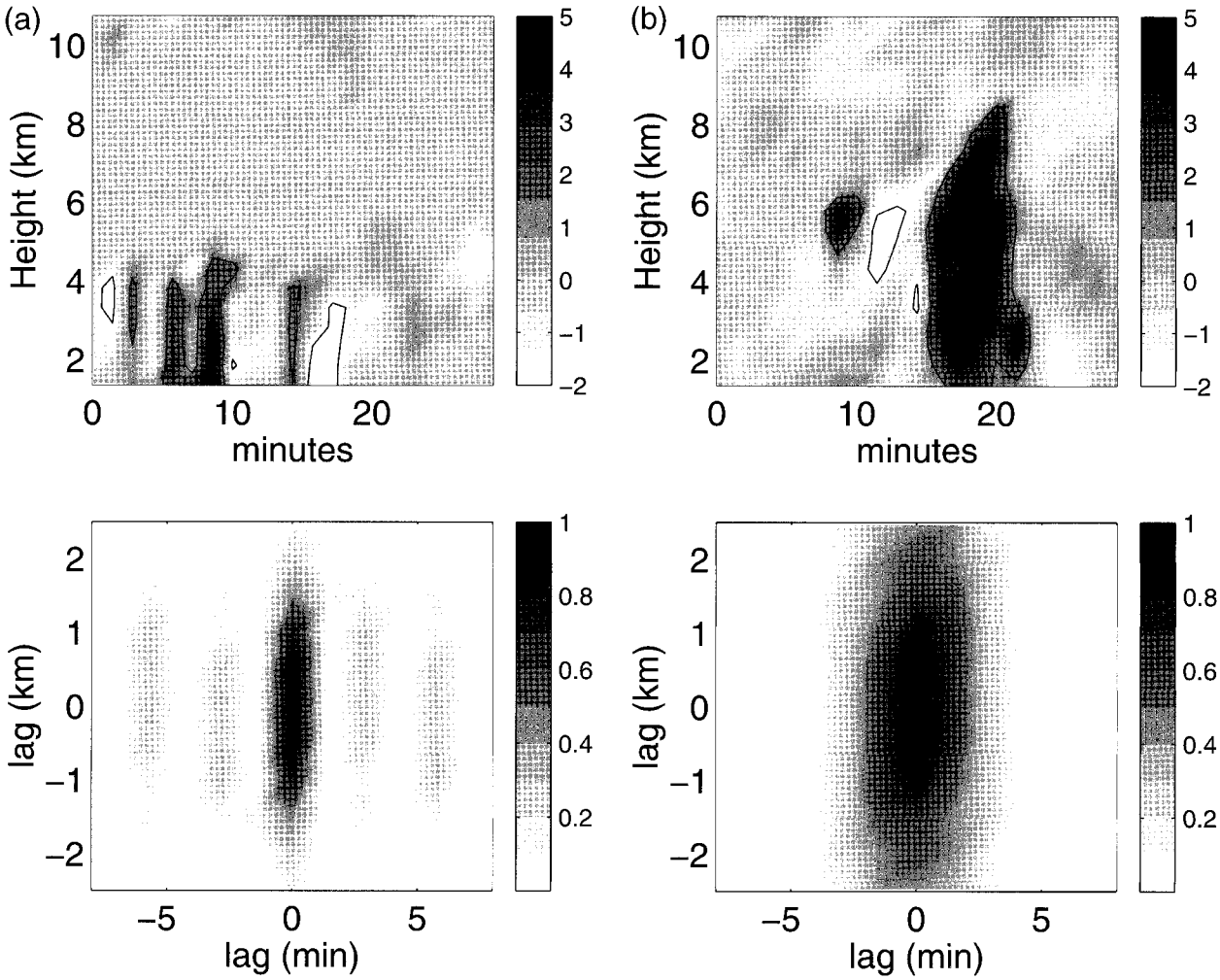

FIG. 3. Time–height sections of vertical velocities (upper) with their corresponding 2D autocorrelation functions lagged in height (km) and time (min) (lower) for (a) case of very shallow organized convection and (b) shallow convection reaching the FZL. The solid lines in the upper panels represent core boundaries.

loading and evaporation producing a cold pool. As the cold pool develops, it may produce a new convergence line and cut off the inflow of high-θ_E air into the mature cell. As noted above, these intense cores often have strong descending motions extending to great heights. The possible origin of upper-level downward cores is complex. Sublimation and condensate loading may contribute in the upper levels (Knupp 1987), but many of these cores are located in weak echo or clear air regions. Other possibilities include a blocking effect (e.g., Lemon and Doswell 1979), but the downdrafts occur on both sides of the upward cores and other studies show complicated relationships between the upward and downward cores (Heymsfield and Schotz 1985; Yuter and Houze 1995a). This suggests that the upper-level cores may be driven, at least in part, by pressure perturbations induced by the strong updrafts (e.g., Yuter and Houze 1995b); that is, many of the downward cores adjacent to the upward cores arise from a dynamical response. These deep downward cores also provide indirect support for the observation of thermally buoyant downdrafts observed by aircraft (Jorgensen and LeMone 1989; Lucas et al. 1994). The pressure perturbations also affect the updrafts themselves (e.g., Trier et al. 1997).

The mature cell has a sloped structure consistent with long-lived convection. However, the autocorrelation functions often have an erect component embedded within the sloping structure. In general, the updrafts tend to be more coherent than downdrafts, and when the up and down motions are correlated separately, the downdrafts tend to be steeper on average. These systems also have the highest coherence. The slope of the correlation functions vary from about 30° to 60° from horizontal, similar to that observed in GATE (LeMone et al. 1984). This is further illustrated by the mean correlation function for all the deep cases (Fig. 6).

The vertical coherence scale is a few kilometers. This is similar to that obtained by Black et al. (1996), where

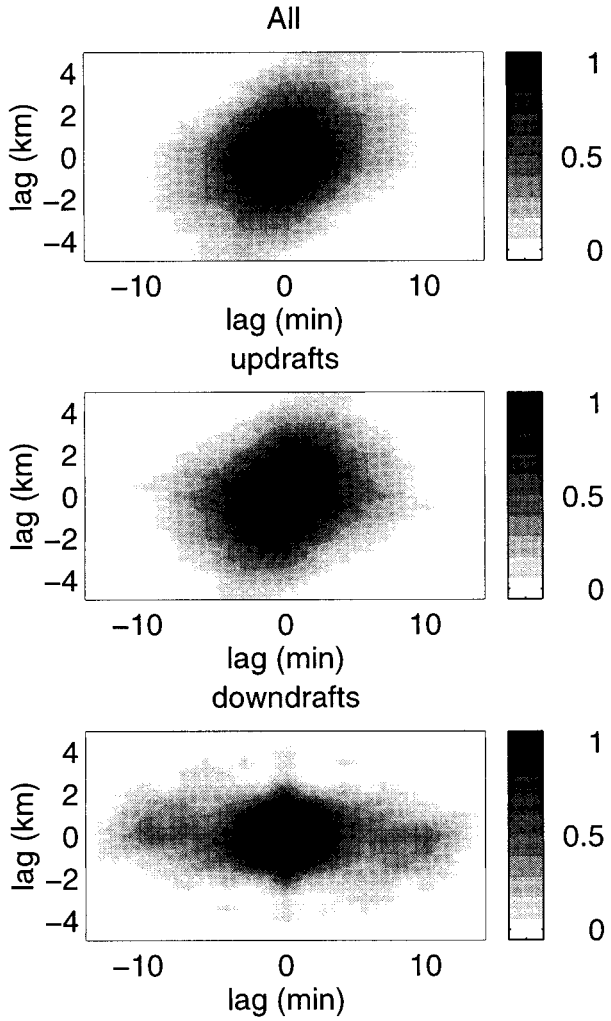

FIG. 4. Two-dimensional autocorrelation function lagged in height (km) and time (min) of all the cases of shallow convection.

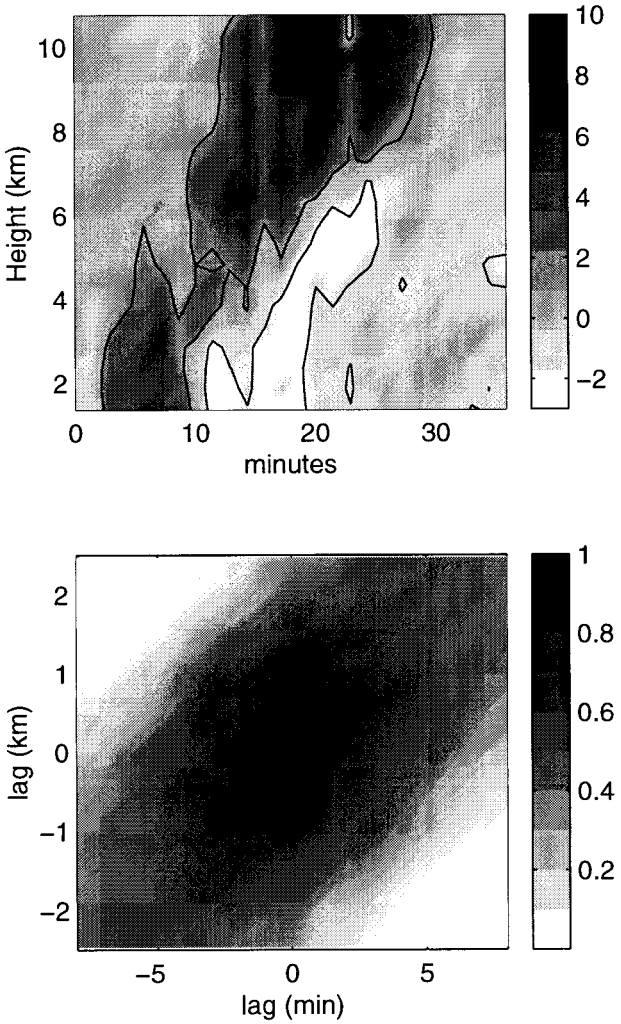

FIG. 5. As in Fig. 3 but for a case of deep convection.

they were correlating the vertical motion at a given height (2.5 and 7.5 km) with the vertical motion at adjacent heights and times. The magnitudes of the correlations are higher here, but this is probably associated with the removal of the ''noise spike'' and renormalization of the correlation coefficients.

These data also capture many cases where the undercutting downdraft appears to have cut off the low-level updrafts altogether (e.g., Fig. 7). In these examples the signature strongly resembles the classic mesoscale up–downdraft couplet often seen in the trailing stratiform regions of squall lines. However, these are still on the spatiotemporal scale of the convective core and contain core amplitudes that exceed 3–4 m s^{-1}. The correlation functions of these systems reflect the limited vertical extent of the sampled cores and a tendency for larger spatial scales. We interpret these cases as examples where the convective cell is collapsing into a stratiform pattern; that is, we are seeing regions where there is a true transition from convective to stratiform rain processes (e.g., Biggerstaff and Houze 1991). There are perhaps more of these cases than would be expected for a truly random sample and may be a reflection of a common life cycle where storms are triggered over elevated terrain to the south and east and are dissipating as they approach Darwin.

The characteristics of these three types were largely seen in the sequence of velocity characteristics during the evolution of a storm complex described by Yuter and Houze (1995b). During the initial development of a storm complex they observed extensive shallow convection and, as the storms matured, a similar acceleration above the FZL. This was followed by a decay into a more stratiform circulation and much reduced velocity variance, similar to our decay cases.

4. Statistical characteristics

Cores have been defined as contiguous measurements with a velocity amplitude greater than 1.5 m s^{-1}. The

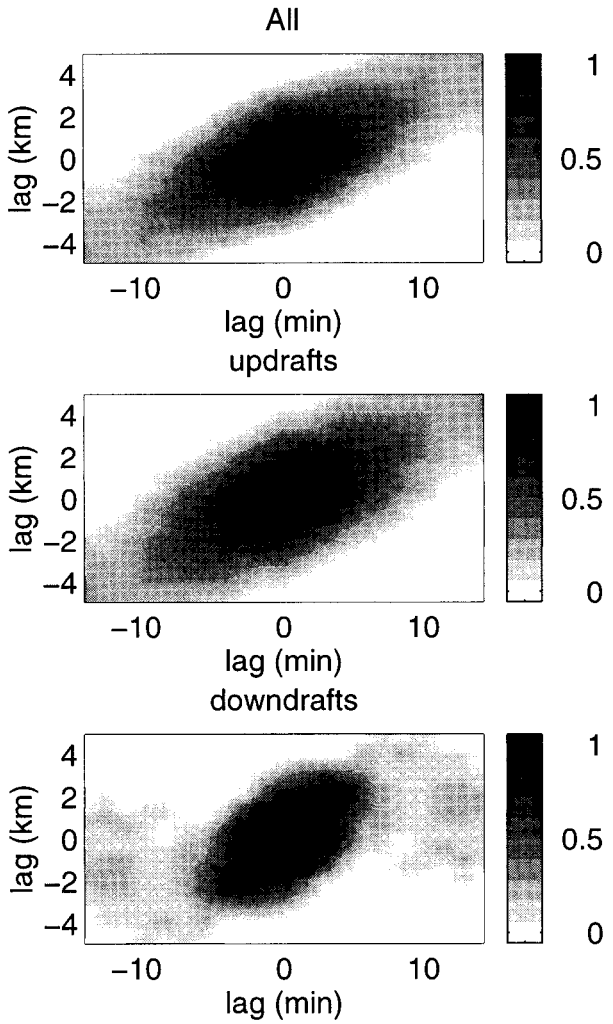

FIG. 6. As in Fig. 4 but for deep convection.

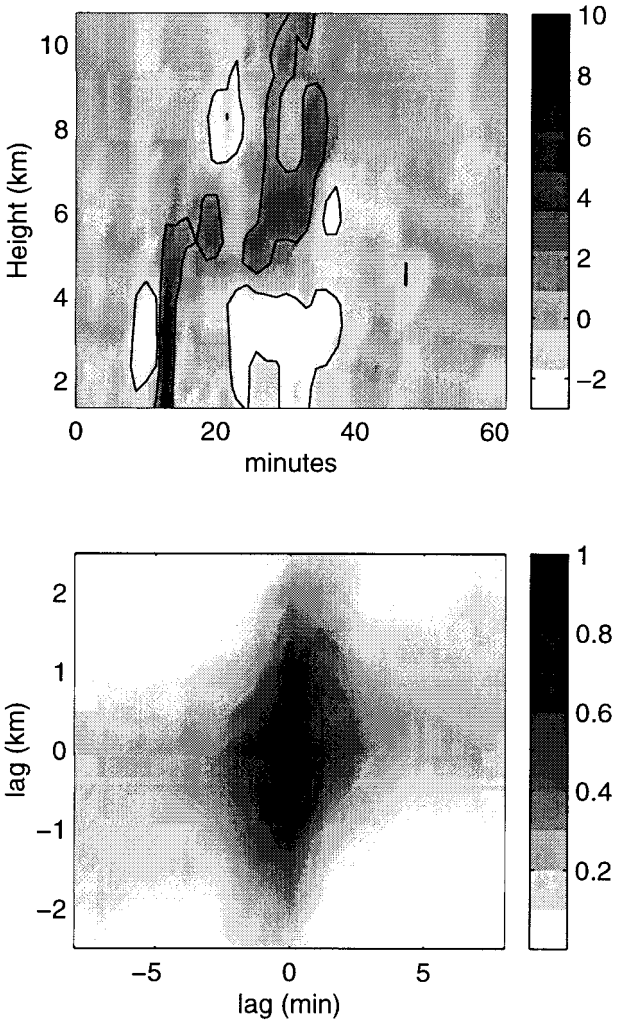

FIG. 7. As in Fig. 3 but for a case of decaying convection.

number of cores at each height for the entire dataset is shown in Fig. 8. The number of upward cores is almost independent of height. However, this does not imply that the cores are coherent through the whole depth. We have seen in the previous section that the cores may be confined over a limited height range as well as merge or split with height. The number of downward cores is constant above the FZL, slightly lower than the number of upward cores, and increases markedly below the FZL. However, there are many coherent downdrafts that do not meet the core magnitude threshold. This data is consistent with our inference that downward cores may be associated with adjustments to the intense upward cores producing a uniform profile with height, with an additional group of downward cores associated with forcing due to precipitation loading and evaporation below the FZL (e.g., Srivastava 1985; Knupp 1987). Note also that the total number of cores is similar to that used by LeMone and Zipser (1980).

While the main emphasis on the remaining discussion

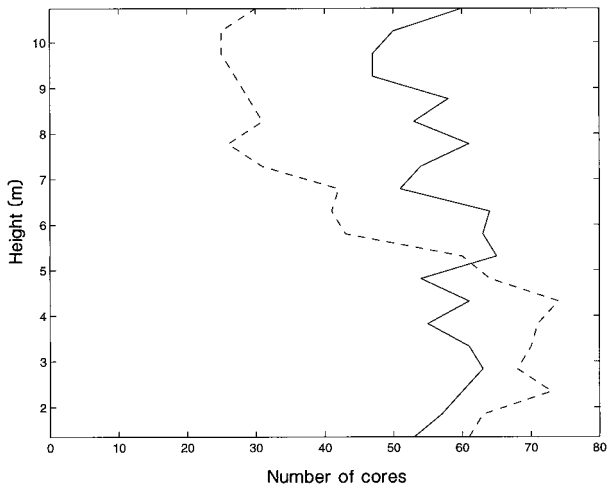

FIG. 8. Numbers of upward (solid) and downward (dashed) cores as a function of height.

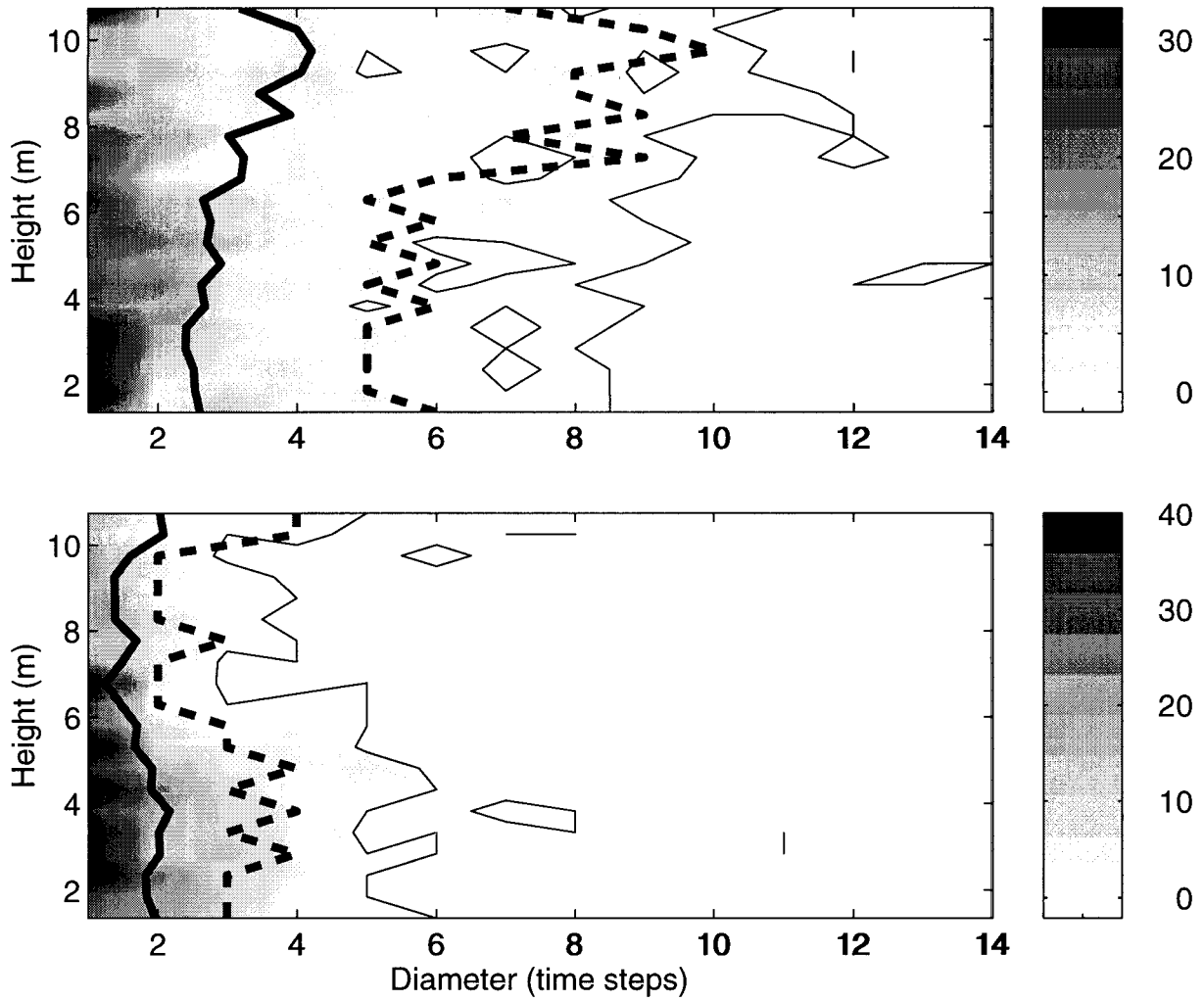

FIG. 9. Histograms of core diameter as a function of height for upward (upper) and downward (lower) cores. The number of points in each sample bin (corresponding to a sampling time of 86 s) is then contoured. The heavy solid and dashed lines are the mean and 90th percentile of the distributions as a function of height. The light solid line marks the boundary of single cases within a bin of the histograms.

is on the statistics of the ensemble of cases, it is worth noting the characteristics of core numbers within the three categories. The shallow cases have the most low-level cores (~½ of the total) and similar numbers of up- and downward cores. The deep cases have a maximum in the number of upward cores just above the FZL, while the decaying cases show a general increase in the number of upward cores with height, and both have more upward than downward cores above the FZL. On the other hand, below the FZL the deep cases have similar numbers of upward and downward cores while the decay cases have a preponderance of downward cores.

a. Core size

Histograms of the core diameters in terms of the 86-s sampling bins have been calculated at each height. If the cores are approximately circular, the estimates of core diameter will be biased low by ~22% (Jorgensen et al. 1985) as the cores will rarely pass directly over the profiler. The temporal scale corresponds to a spatial sampling scale of about 800 m, assuming the storms translate on average at a speed slightly less than 10 m s^{-1} (the results using a time–space conversion based on the 700-hPa wind are similar). The estimates of core diameter are highly quantized. These histograms are plotted as contours versus height (Fig. 9) in a similar display to the contoured frequency by altitude diagrams of Yuter and Houze (1995b), except that in this case the absolute numbers of cases are plotted. This is so that changes in the numbers of cores with height are represented. Also plotted are the mean core diameters and the 90th percentile limit as a function of height.

As expected, most of the cores are small, but large cores exceeding a duration of 10 min are seen at all heights. The upward cores show a tendency to slightly increase in size on average and the 90th percentile in-

creases by about 50% from 2 to 10 km. The downward cores have a marked increase in diameter below the FZL, as may be expected from previous arguments. However, an increase is also seen at the highest levels analyzed. We speculate that this may be associated with the increasing diameter of the upward cores and the decreasing air density with height.

The statistical distribution of the core diameters has been tested against exponential and lognormal distributions. In general, the data fits a lognormal distribution reasonably well, consistent with the results of Lopez (1976, 1977), Houze and Cheng (1977), and LeMone and Zipser (1980) from GATE and the hurricane data examined by Black et al. (1996).

b. Core velocities

A similar histogram-based analysis has been performed for the mean and maximum velocities within the cores (Fig. 10). Sampling issues again imply that our velocity estimates are biased, but for a circularly symmetric core with a triangular velocity profile, the bias of the mean velocity within the core is only about 10% but is a factor of 2 for the maximum velocity. The distributions are again dominated by weak cores and again the distributions are quite close to being lognormal. The height profile of the mean and 90th percentile of the upward mean velocities is fairly constant, with some indication of a weak peak just below the FZL associated with the shallow cases. Overall, there is a tendency to increase with height. The core maximum velocity is, of course, much more spread out and reaches higher peak values (although the mean does not change much) with height. The downward cores again show a structure of acceleration below the FZL and some indication of stronger motions at the uppermost levels. Peak velocities greater than 15 m s^{-1} averaged over the 86-s interval have been recorded at the upper levels and over 8 m s^{-1} below the FZL.

The time series of individual core velocities tends to be triangular in shape, rather than a ''top hat'' section. This finding is consistent with numerous aircraft (e.g., LeMone and Zipser 1980; Zipser and LeMone 1980) and profiler observations (Cifelli and Rutledge 1994; May and Rajopadhyaya 1996). This is in evidence in both individual time series and in a statistical sense where the ratio of the mean and maximum velocities is approximately $w \sim (w\text{max} + 1)/2$.

The mean velocity within the upward cores is slightly correlated with the core diameter (correlations ~0.4–0.5) with some evidence of a decrease above the FZL, while the downward cores are slighly less correlated below the FZL and not significantly correlated at all above the FZL. Again, these results are broadly consistent with those of Zipser and LeMone (1980).

c. Core mass fluxes

The mass flux within a core is the product of the air density ρ, mean velocity within the core w, and its duration ΔT:

$$F = \rho w \Delta T.$$

The mass flux histograms are dominated by small, weak cores and are again approximately lognormally distributed. However, this does not describe what scales carry the most mass flux. This is investigated in two ways. The first is to examine the mass flux distribution with respect to mean velocity and the second is to look at the contributions to the first moment of the mass flux histograms as a function of mass flux. The first moment is defined as the integral of $F \times$ the number of cores per F interval as a function of the F per core. The peak of the distributions shows the characteristic mass flux responsible for carrying the most total flux; for example, it takes 10 times as many weak cores to carry the same total flux as a single core with 10 times the flux, and each would have the sample amplitude (i.e., make the same contribution to the first moment) in the moment distributions.

Figure 11 shows the distribution of total mass flux associated with cores in the dataset as a function of mean core velocity. In the case of the upward mass flux, the distribution is quite wide. The peak in the distribution is associated with velocities of about 2–3 m s^{-1} in the lower heights, but the velocity of the peak increases almost linearly with height, so that at the upper levels the mass flux is associated with stronger cores: those with mean velocities of ~5–6 m s^{-1}. The first moment distribution (Fig. 12) confirms the view that many scales are important in the mass flux budget. A peak is still visible for smaller mass flux cores, but significant contributions extend to cores with large mass fluxes. The dominant temporal scales carrying the upward mass flux increases with height, but spatial scales from ~1 km to more than 10 km are all important. The wide range of important scales has important implications. The most intense cores have been most commonly studied, while Yuter and Houze (1995c) showed that in some cases the smaller scales in fact carried the bulk of the mass flux by virtue of their larger numbers. These data suggest that the mass flux is carried by a wide range of spatial and velocity scales and all are important.

The situation with downward cores is quite different. Here the small/weak cores dominate the mass flux through sheer numbers, although it is apparent that the dominant scale increases substantially below the FZL. This tendency is also true of the dominant spatial scale carrying downward mass flux.

5. Summary statistics

Mass flux profiles compiled over the entire dataset along with the total flux within the shallow, deep, and

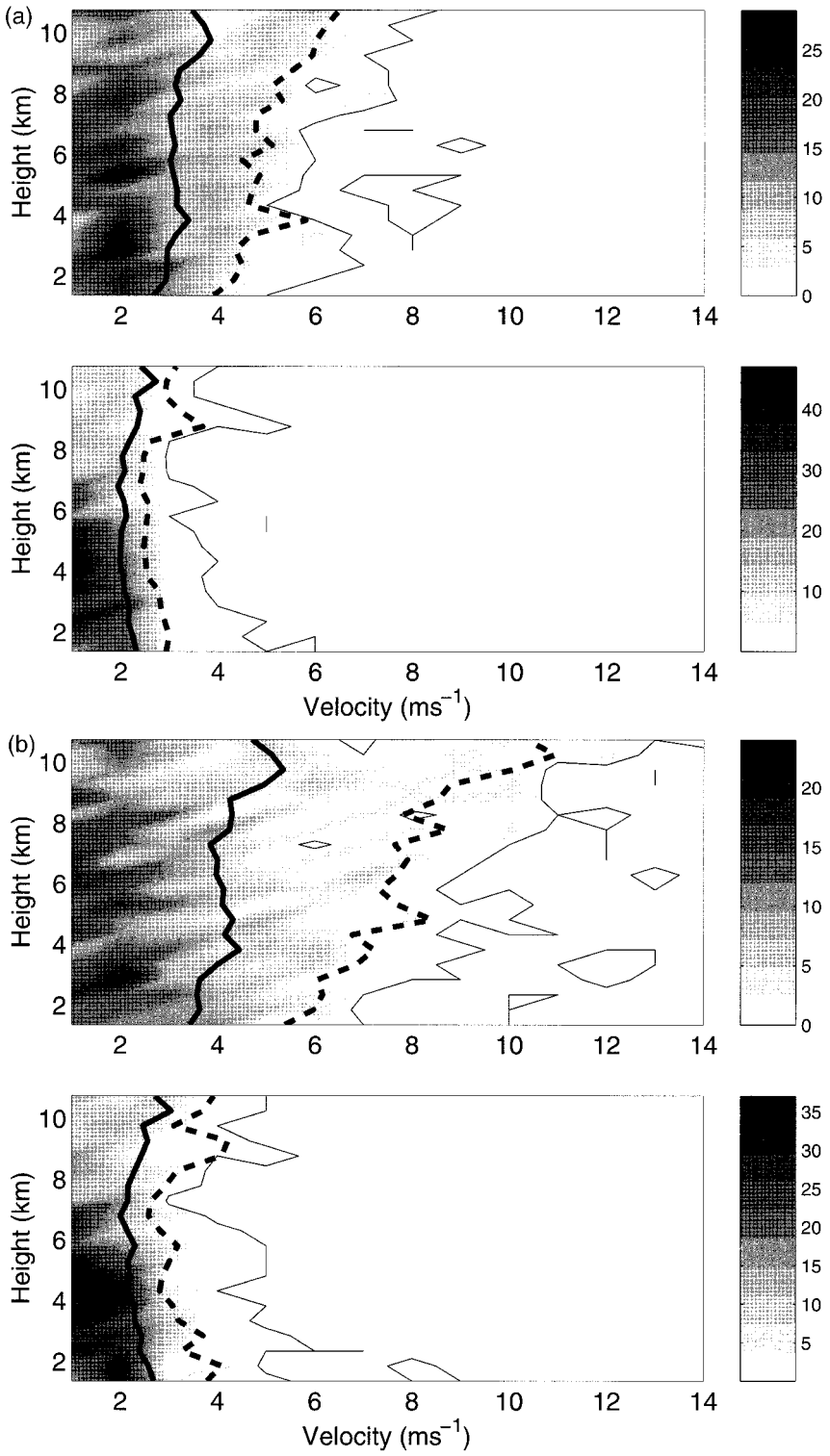

FIG. 10. As in Fig. 9 but for (a) mean and (b) maximum velocities. The histograms were calculated using intervals of 1 m s^{-1}.

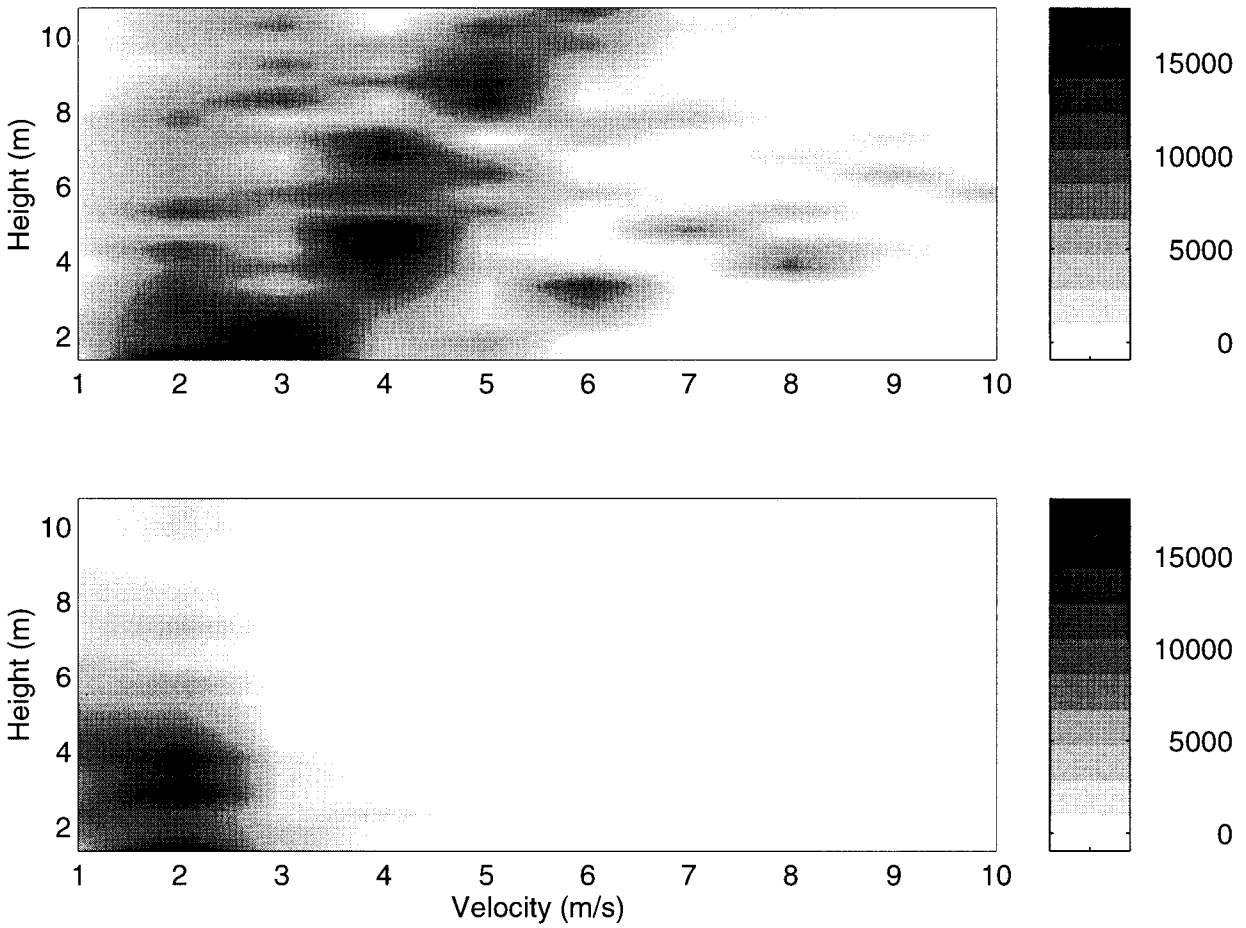

FIG. 11. Distribution of total mass flux within cores as a function of mean core velocity and height.

decaying systems are shown in Fig. 13. The mean profile associated with upward and downward cores along with their sum and the total flux are all shown. The small low-level mean velocities reflect the near cancellation of the large upward core mean and the sum of the near environment and downward cores below the FZL. Interestingly, the near environment contributes a similar amount to the total downward flux as the cores themselves. Despite the increase in size and mean velocity of the upward cores with height, the mass flux is almost uniform below the FZL and actually decreases with height, showing an average detrainment of the buoyant air. This net detrainment is associated with cores with both large and small horizontal dimensions. The profile of the total mean velocity (not shown) is similar in shape to that observed by Balsley et al. (1988), although the amplitude here is about one-third of their observations. This is because of the way data have been selected: here all data near cores are selected while Balsley et al. stratified their data according to rain rates greater than 2.54 mm h^{-1}.

There is a difference in the mean core velocity if the profiler data is stratified into monsoonal and break regimes with the break data 0.5–1 m s^{-1} more intense up to about 6 km. This is consistent with the results of Cifelli and Rutledge (1993). This is partly a product of there being no shallow cases in the monsoon season, possibly associated with more intense sea-breeze circulations during the break. However, there is an indication in the time–height cross sections that the deep break systems have more shallow convection ahead of the deep circulations (consistent with initiation on the cold pool outflow), indicating that the environmental shear may also be playing a role.

The downward cores show a dramatic increase in downward mass flux below the FZL associated with melting. This is no surprise as both the core velocities and size increased associated with evaporation and the onset of significant precipitation loading (Figs. 9, 10). The upper-level maximum in downward mean velocity seen in Fig. 10 is weak and does not offset the decreasing density with height and, thus, is not reflected by a mass flux maximum.

The total mass flux is slightly downward in the lowest 2 km. If the systems are separated into shallow, deep, and decaying systems using the loose definition that

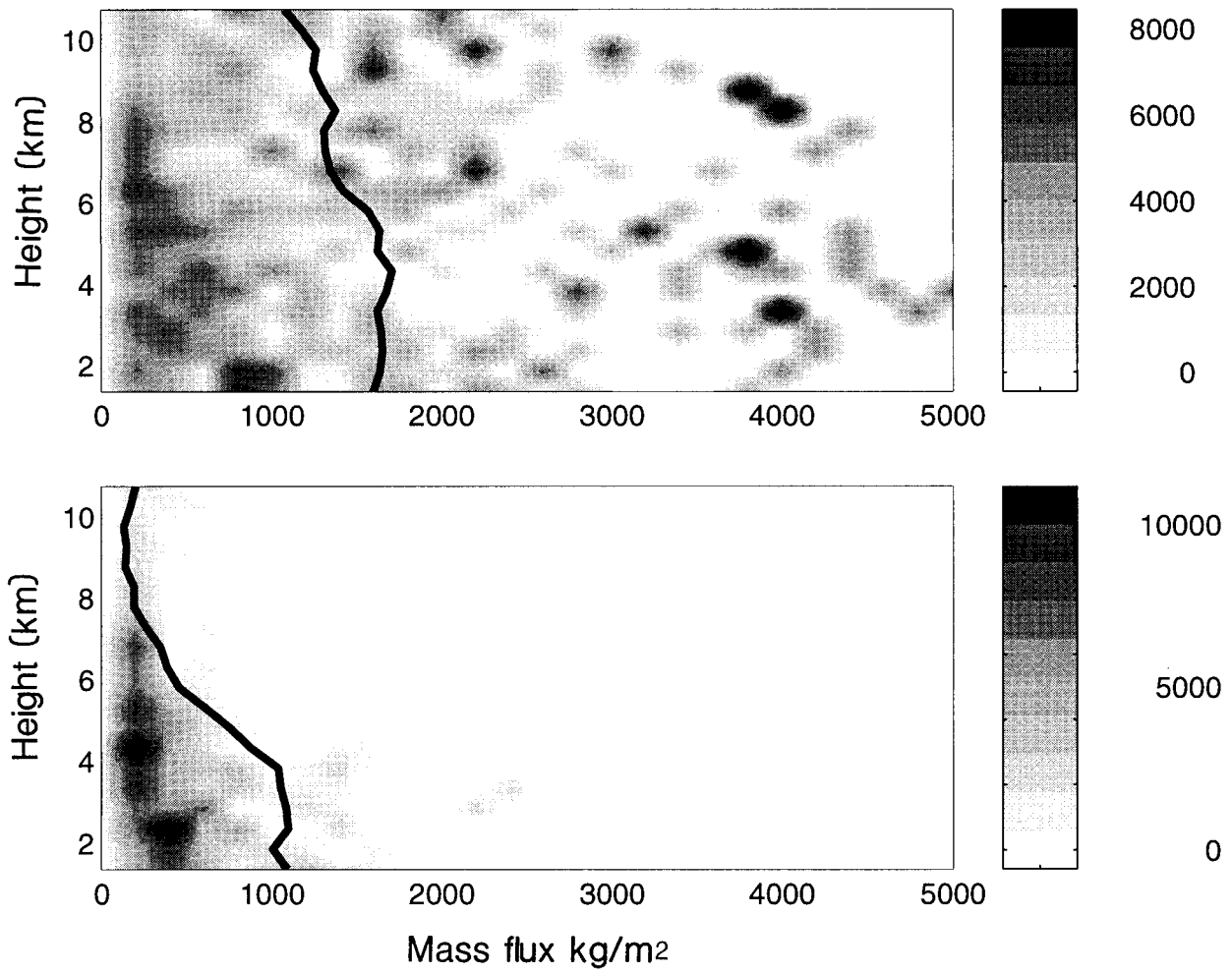

FIG. 12. Distributions of the product of the mass flux within a core by the number of cores, which shows the contributions to the first moment of the mass flux distributions as a function of mass flux within cores. The peak of the distributions show the characteristic mass flux per core responsible for carrying the most total flux. The mean is marked by the solid line.

decaying systems show a more stratiform-like circulation, it is easily seen that this downward velocity is associated with the decaying systems. This also illustrates the importance of the shallow systems to the overall mass balance. However, it is often the case that storms are generated over higher terrain to the south and east of the profiler and are in the final stages of their life cycle as they approach Darwin (Keenan and Carbone 1992). This is represented in this dataset by the presence of several decaying systems. Thus, the overall downward mass flux at lower levels is probably an artifact of the mixture of storm life cycle effects and the large number of decaying systems in the sample into the dataset.

6. Comparison with aircraft observations

Lucas et al. (1994) presented a summary of the size/intensity of the largest/most intense 10% of cores observed in the GATE, EMEX, Taiwan Area Mesoscale Experiment (TAMEX), and Thunderstorm Project (TP) datasets, as well as a summary based on hurricane eyewall and rainband penetrations by reconnaissance aircraft. Of particular relevance here are the estimates of core dimensions and mean vertical motions within the cores. These data, with the exception of the TP, are all tropical oceanic convection and provide an ideal comparison with the characteristics of the mostly continental convection sampled by the profiler.

A comparison of the amplitude of the vertical motions within cores is straightforward, but in order to compare scale sizes estimated from aircraft and the time sections from the profiler the time-to-space scale discussed in section 2 is used. Cores with an estimated diameter of less than 1 km were excluded for consistency with the aircraft definitions. The coarse quantization of the profiler sampling remains another source of discrepancy.

Figure 14 shows the 90th percentile of the core diameter distributions for the experiments. There is considerable variability from study to study with the Dar-

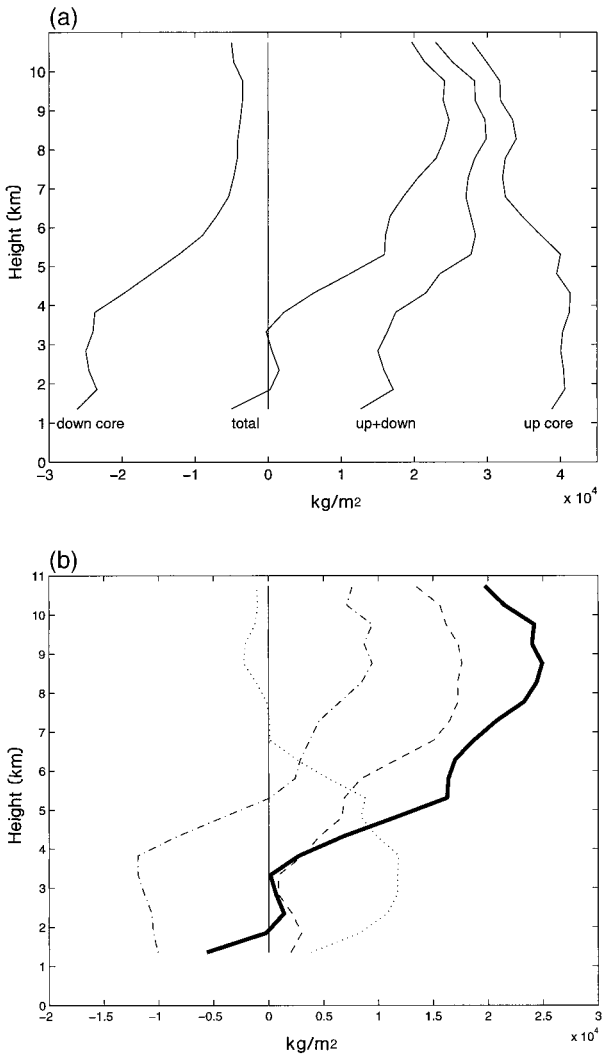

FIG. 13. (a) Profiles of the mass flux in the downward cores, upward cores, flux within all the cores, and the total mass flux within the periods under consideration for the total period of 33 h; (b) profiles of the total mass flux for the shallow (dotted), deep (dashed), decaying (dash–dotted), and all the cases (heavy solid).

win data, the eyewall and TP diameters having similar and larger scales than the remaining oceanic cases for both up- and downdrafts. There tends to be comparatively little vertical structure in the diameters over these heights except for the EMEX and eyewall upward cores increasing with height. Furthermore, it is apparent in the data that the continental profiler cases have larger core diameters below the FZL than the (small sample of) oceanic monsoon cases. These results are consistent with an association between core size and boundary layer depth (Lucas et al. 1996). The only aircraft data to extend much above the FZL are from the TP, and the difference in the downdraft vertical structure is significant, with the downward cores increasing in diameter with height quite rapidly while the Darwin data actually decrease slightly. There is also some evidence of stratification in the core sizes of the oceanic and continental core diameters.

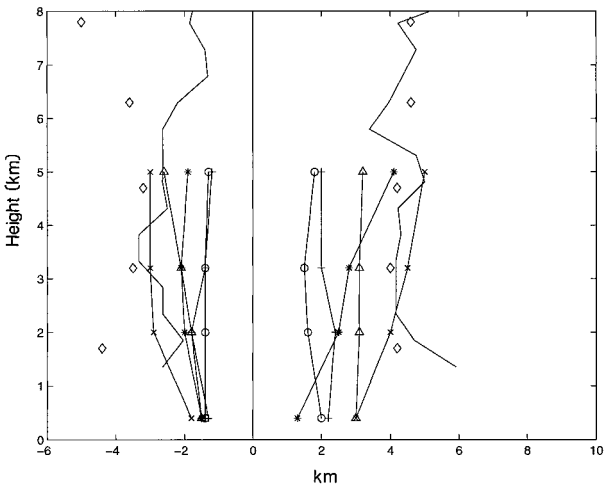

FIG. 14. Comparisons of the largest 10% of core diameters for GATE (○– – –○), TAMEX (+– – –+), EMEX (*– – –*), hurricane eyewall penetrations (×– – –×), hurricane rainbands (△– – –△), the Thunderstorm Project (◊), and the Darwin profiler data (solid lines), where downward cores have negative diameters (aircraft data adapted from Lucas et al. 1994).

Figure 15 shows the 90th percentile of the mean vertical motion distributions (i.e., the most intense 10% of the cores) in the above experiments. There is a remarkable similarity in all the profiles except the hurricane rainbands and the TP data. The weakness of the rainband cores is not surprising since there is generally very little CAPE in rainband soundings, as the profiles are almost moist adiabatic (e.g., Frank 1977). The agreement between the oceanic and continental tropical statistics is surprising, as there is evidence to suggest that the continental upward cores should be more intense. There is some evidence that the maximum upward velocities are larger, but the difference in sampling [1-s sampling in

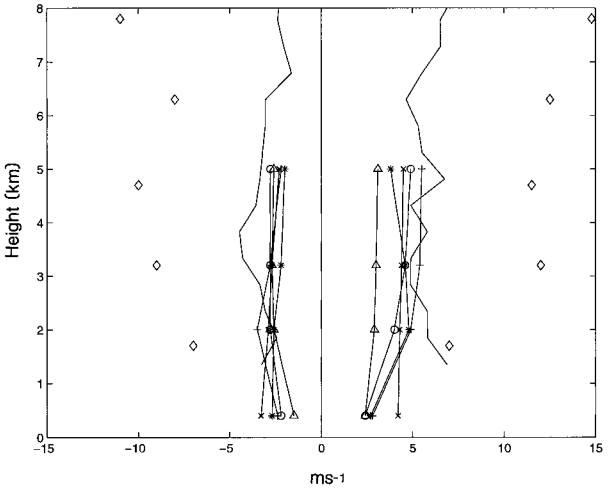

FIG. 15. As in Fig. 14 but for the mean velocity in the cores.

an aircraft at ~100 m vs 86 s (~700 m) for the profiler] makes this suggestive rather than definite. In contrast, all the data are much weaker than the TP data. This lends some support to the hypothesis by Lucas et al. (1994) that the difference is due to the vertical distribution of CAPE over a much greater depth in the Tropics. In the Tropics, the acceleration is over a much greater depth so that there is more chance for mixing and entrainment of environmental air decreasing the maximum velocities. There is also more precipitation loading compared with the available CAPE below the FZL in the Tropics, limiting the magnitudes of the upward cores. Thus, there is less net buoyancy and precipitation loading can have more effect. However, another factor to consider is that some systematic life cycle effects are mixed into this dataset, so the mean upward core velocity may be larger to the east of Darwin. Observations in other locations and greater heights may also produce more intense cores (e.g., Simpson et al. 1993).

The downward cores in all of the datasets are again similar with the exception of the TP data. This may be related to the higher rainfall rates, or a dynamical response to the larger amplitude of the upward cores in the TP data.

The larger core sizes in the profiler dataset along with similar mean values combine to give significantly more mass flux in the strong cores in the profiler dataset compared with the oceanic data, except again the eyewall data. Note also that both the core diameter and mean velocity profiles do not change much over the heights sampled by the profiler, but as shown in Fig. 10, the maximum velocities within the upward cores do increase almost linearly with altitude.

7. Conclusions

Three types of systems have been identified with clearly distinguishable characteristics. There are shallow cases with warm rain processes dominating and a vertically erect structure, deep glaciated cells with well-defined convective downdrafts, and a highly tilted draft structure and decaying systems that are transitioning into a stratiform-type circulation. All three are important in the overall mass flux distributions and the shallow systems may exist in close proximity to the other two. The characteristics here were predominantly during wind conditions suggesting continental convection. However, the characteristics in other areas, such as over the Tiwi Islands north of Australia (e.g., Simpson et al. 1993) may well be quite different.

This analysis of wind profiler data has shown many similarities with aircraft measurements, but with the added capability of observations over a deep layer. The statistical characteristics of the vertical motions show a similar lognormal distribution. The similarity between the mean vertical motion observed in all the tropical locations is a strong indication that the most intense cores are mostly limited by the available CAPE at a given height. This supports the assertion by Lucas et al. (1994) that the tropical motions are smaller than the midlatitudes because the CAPE is spread over a much deeper layer,so that there are smaller temperature differences between parcels and their environment at a given level. They suggested that this allows more detrainment, but on average, the upward cores detrain mostly above the FZL. This occurs at a similar rate regardless of horizontal scale. The size of the cores, however, is significantly greater here compared with oceanic data and is consistent with midlatitude results, thus supporting the suggestion that boundary layer depth is important in determining the horizontal scales (Lucas et al. 1996). The maximum velocity within cores tends to increase with height, as expected as more CAPE can be released. Examples of velocities greater than 15 m s^{-1} were seen, but the maximum height for data in this study was 11 km. Together with the temporal–spatial averaging of this data, these results are consistent with very large amplitude motions in the upper troposphere in intense convection in the area (e.g., Simpson et al. 1993).

Two distinct populations of downdrafts are inferred. A precipitation/evaporatively driven downdraft (e.g., Srivastava 1985) is dominant below the FZL. At all heights, downdrafts are seen next to the most intense upward cores. These appear to be dynamically driven (Knupp 1987; Yuter and Houze 1995b). The number of these is almost uniform with height on either side of the FZL, as is the number of upward cores at all heights. Together with the almost constant number of upward cores as a function of height, this suggests that the number of dynamically driven downdrafts are almost uniform in height. Assuming that most of the upper-level downward cores are dynamically driven, this means that approximately two-thirds of the downward cores below the FZL are buoyancy driven.

Well-defined strong low-level vertically erect cores in shallow cases contribute significantly to overall mass flux, indicating the importance of warm rain processes. The total downward mass flux at low heights is probably an artifact of an overrepresentation of decaying systems observed in the area (Keenan and Carbone 1992). The total mass flux below the FZL is small because of cancellation of large terms producing an upper-level heating maximum consistent with radiosonde budgets (e.g., Yanai et al. 1973; Frank and McBride 1989). It was seen that a wide range of spatial and velocity scales contribute to the mass flux in upward cores, while the dominant downward flux was in small cores.

Acknowledgments. Many thanks to C. Lucas of Texas A&M University for supplying the summary aircraft statistics used in this paper. Many people have made useful comments during talks describing this work. The comments of the reviewers, Drs. M. LeMone, S. Trier, and E. Zipser have greatly improved the paper. This work was partly performed while P. May was visiting

CIRES at the University of Colorado under NASA Contract NAGW-4146.

REFERENCES

Balsley, B. B., W. L. Ecklund, D. A. Carter, A. C. Riddle, and K. S. Gage, 1988: Average vertical motions in the tropical atmosphere observed by a radar wind profiler on Pohnpei (7°N latitude, 157°E longitude). *J. Atmos. Sci.,* **45,** 396–405.

Biggerstaff, M. I., and R. A. Houze Jr., 1991: Kinematic and precipitation structure of the 10–11 June 1985 squall line. *Mon. Wea. Rev.,* **119,** 3035–3065.

Black, M. L., R. W. Burpee, and F. D. Marks Jr., 1996: Vertical motion characteristics of tropical cyclones determined with airborne Doppler radial velocities. *J. Atmos. Sci.,* **53,** 1887–1909.

Byers, H. R., and R. R. Braham, 1949: The Thunderstorm Project. U.S. Department of Commerce Tech. Rep., 287 pp. [NTIS PB234515.]

Chilson, P. B., C. W. Ulbrich, M. F. Larsen, P. O. Perillat, and J. E. Keener, 1993: Observations of a tropical thunderstorm using a vertically pointing, dual-frequency collinear beam Doppler radar. *J. Atmos. Oceanic Technol.,* **10,** 663–673.

Cifelli, R., and S. A. Rutledge, 1994: Vertical motion structure in Maritime Continent mesoscale convective systems: Results from a 50-MHz profiler. *J. Atmos. Sci.,* **51,** 2631–2652.

——, and ——, 1998: Vertical motion, diabetic heating, and rainfall characteristics in N. Australia convective systems. *Quart. J. Roy. Meteor. Soc.,* **124,** 1133–1162.

Drosdowsky, W., 1996: Variability of the Australian summer monsoon at Darwin: 1957–1992. *J. Climate,* **9,** 85–96.

Frank, W. M., 1977: The structure and energetics of the tropical cyclone. I. Storm structure. *Mon. Wea. Rev.,* **105,** 1119–1135.

——, and J. L. McBride, 1989: The vertical distribution of heating in AMEX and GATE cloud clusters. *J. Atmos. Sci.,* **46,** 3464–3478.

Fukao, S., K. Wakasugi, T. Sato, S. Morimoto, T. Tsuda, I. Hirota, I. Kimura, and S. Kato, 1985: Direct measurement of air and precipitation particle motion by very-high-frequency Doppler radar. *Nature,* **316,** 712–714.

Gray, W. M., 1965: Calculations of cumulus vertical draft velocities in hurricanes from aircraft observations. *J. Appl. Meteor.,* **4,** 463–474.

Heymsfield, G. M., and S. Schotz, 1985: Structure and evolution of a severe squall line over Oklahoma. *Mon. Wea. Rev.,* **113,** 1563–1589.

Holland, G. J., 1986: Interannual variability of the Australian summer monsoon at Darwin: 1952–1982. *Mon. Wea. Rev,* **114,** 594–604.

Houghton, H. G., 1968: On precipitation mechanisms and their artificial modification. *J. Appl. Meteor.,* **7,** 851–859.

Houze, R. A., Jr., 1981: Structures of atmospheric precipitation systems: A global survey. *Radio Sci.,* **16,** 671–689.

——, and C. P. Cheng, 1977: Radar characteristics of tropical convection observed during GATE: Mean properties and trends observed over the summer season. *Mon. Wea. Rev.,* **105,** 964–980.

Jorgensen, D. P., and M. A. LeMone, 1989: Vertical velocity characteristics of oceanic convection. *J. Atmos. Sci.,* **46,** 621–640.

——, E. J. Zipser, and M. A. LeMone, 1985: Vertical motions in intense hurricanes. *J. Atmos. Sci.,* **42,** 839–856.

Keenan, T. D., and R. E. Carbone, 1992: A preliminary morphology of precipitation systems in tropical northern Australia. *Quart. J. Roy. Meteor. Soc.,* **118,** 283–326.

Knupp, K. R., 1987: Downdrafts within High Plains cumulonimbi. Part I: General kinematic structure. *J. Atmos. Sci.,* **44,** 987–1008.

Kuettner, J. P., P. A. Hildebrand, and T. L. Clark, 1987: Convection waves: Observations of gravity wave systems over convectively active boundary layers. *Quart. J. Roy. Meteor. Soc.,* **113,** 445–467.

Larsen, M. F., and J. Rottger, 1987: Observations of thunderstorm reflectivities and Doppler velocities measured at VHF and UHF. *J. Atmos. Oceanic Technol.,* **4,** 151–159.

Lemon, L. R., and C. A. Doswell III, 1979: Severe thunderstorm evolution and mesocyclone structure as related to tornadogenesis. *Mon. Wea. Rev.,* **107,** 1184–1197.

LeMone, M. A., and E. J. Zipser, 1980: Cumulonimbus vertical velocity events in GATE. Part I: Diameter, intensity and mass flux. *J. Atmos. Sci.,* **37,** 2444–2457.

——, G. A. Barnes, E. J. Szoke, and E. J. Zipser, 1984: The tilt with height of the leading edge of a tropical mesoscale convective line. *Mon. Wea. Rev.,* **112,** 510–519.

Lopez, R. E., 1976: Radar characteristics of the cloud population of tropical disturbances in the northwest Atlantic. *Mon. Wea. Rev.,* **104,** 268–283.

——, 1977: Some properties of convective plume and small fair weather cumulus fields as measured by acoustic and lidar sounders. *J. Appl. Meteor.,* **16,** 861–865.

Lucas, C., E. J. Zipser, and M. A. LeMone, 1994: Vertical velocity in oceanic convection off tropical Australia. *J. Atmos. Sci.,* **51,** 3183–3193.

——, ——, and ——, 1996: Reply. *J. Atmos. Sci.,* **53,** 1212–1214.

Malkus, J. S., 1955: On the formation and structure of downdrafts in cumulus clouds. *J. Meteor.,* **12,** 350–354.

May, P. T., 1991: Recent developments and performance of radar wind profilers and RASS. *Aust. Meteor. Mag.,* **39,** 237–245.

——, and D. K. Rajopadhyaya, 1996: Wind profiler observations of vertical motion and precipitation microphysics of a tropical squall line. *Mon. Wea. Rev.,* **124,** 621–633.

——, and ——, 1997: Corrigendum. *Mon. Wea. Rev.,* **125,** 410–413.

——, W. L. Ecklund, and G. D. Hess, 1995: Spectral and bispectral characteristics of wind variability at Darwin, Australia observed by a VHF radar wind profiler. *Quart. J. Roy. Meteor. Soc.,* **121,** 527–544.

Rasmussen, E. N., and S. A. Rutledge, 1993: Evolution of quasi-two-dimensional squall lines. Part I: Kinematic and reflectivity structures. *J. Atmos. Sci.,* **50,** 2584–2606.

Rutledge, S. A., E. R. Williams, and T. D. Keenan, 1992: The Down Under Doppler and Electricity Experiment (DUNDEE): Overview and preliminary results. *Bull. Amer. Meteor. Soc.,* **73,** 3–16.

Simpson, J., T. D. Keenan, B. Ferrier, R. H. Simpson, and G. J. Holland, 1993: Cumulus mergers in the maritime continent region. *Meteor. Atmos. Phys.,* **51,** 73–99.

Srivastava, R. C., 1985: A simple model of evaporatively driven downdraft application to microburst downdraft. *J. Atmos. Sci.,* **42,** 1004–1023.

Trier, S. B., W. C. Skamarock, and M. A. LeMone, 1997: Structure and evolution of the 22 February 1993 TOGA COARE squall line: Organization mechanisms inferred from numerical simulation. *J. Atmos. Sci.,* **54,** 386–407.

Wakasugi, M., A. Mizutani, M. Matsuo, S. Fukao, and S. Kato, 1986: A direct method for deriving drop-size distribution and vertical air velocities from VHF Doppler radar spectra. *J. Atmos. Oceanic Technol.,* **3,** 623–629.

Yanai, M. S., S. Esbenson, and J. H. Chu, 1973: Determination of the bulk properties of tropical cloud clusters from large-scale heat and moisture budgets. *J. Atmos. Sci.,* **30,** 611–627.

Yuter, S. E., and R. A. Houze Jr., 1995a: Three-dimensional kinematic and microphysical evolution of Florida cumulonimbus. Part I: Spatial distribution of updrafts, downdrafts, and precipitation. *Mon. Wea. Rev.,* **123,** 1921–1940.

——, and ——, 1995b: Three-dimensional kinematic and microphysical evolution of Florida cumulonimbus. Part II: Frequency distributions of vertical velocity, reflectivity, and differential reflectivity, *Mon. Wea. Rev.,* **123,** 1941–1963.

——, and ——, 1995c: Three-dimensional kinematic and microphysical evolution of Florida cumulonimbus. Part III: Vertical mass transport, mass divergence, and synthesis. *Mon. Wea. Rev.,* **123,** 1964–1983.

Zipser, E. J., and M. A. LeMone, 1980: Cumulonimbus vertical velocity events in GATE. Part II: Synthesis and model core structure. *J. Atmos. Sci.,* **37,** 2458–2469.